A MATHEMATICAL MODEL FOR A COMPREHENSIVE APPROACH TO THE DYNAMICS OF HUMAN COLONIC ABERRANT CRYPT FOCI

ISABEL N. FIGUEIREDO, PEDRO N. FIGUEIREDO, CARLOS LEAL
AND JOSÉ MIGUEL URBANO

ABSTRACT: In this paper, we propose mathematical models for the growth dynamics of aberrant crypt foci in the human colon, as well as for some of their characteristics, namely the apoptosis and proliferation indices. The models rely on logistic type differential equations and clinical observations at different times, and can arguably be used as an auxiliary screening tool for colon cancer. We report several results using available medical data.

KEYWORDS: Aberrant crypt foci, logistic differential equation, apoptosis index, proliferation index, colorectal cancer.

1. Introduction

Colorectal cancer is one of the most frequent types of malignant tumors in the world and the first leading cause of cancer related death in Portugal. Unlike most other malignancies, it is possible to prevent colorectal cancer. This is due to the long period of time elapsed between the appearance of an adenoma (a benign epithelial tumor) and the eclosion of the carcinoma, which allows for the detection and removal of the benign lesion. In this context, Aberrant Crypt Foci (ACF in short) may have a crucial and determinant role. These are clusters of aberrant (deviant from normal) crypts (small pits, which are compartments of cells, in the colonic epithelium) that are thought to be the precursors of colorectal cancer (cf. [6], [7]). It is necessary to identify features in the ACF that allow doctors to predict which will evolve to neoplasia, so that when they are detected in an individual it can be possible not only to predict what is the risk of presenting an adenoma in the future, but also to adopt screening procedures. Therefore, the time evolution of ACF is a challenging issue of crucial importance.

In this paper, we propose mathematical models for the growth dynamics of ACF and some of their characteristics, more precisely the rate of apoptotic and proliferative cells in ACF. They consist of logistic type differential

equations and aim at simulating the dynamics of ACF. Using only one or two clinical observations these models anticipate the likely growth dynamics of the overall population of ACF and the values of the apoptosis and proliferation indexes in ACF for a large time.

This type of mathematical models seems adequate for the simulation of the dynamics of ACF, and of the apoptosis and proliferation indexes in ACF, if we think of a large scale of time. To clarify this assertion we give now a more detailed explanation of what normal and aberrant crypts are. A normal crypt is a cylindrical tube (with an opening in the top, directed at the lumen's colon) that contains different populations of cells. These are aligned along the crypt wall: stems cells are believed to reside in the bottom of the crypt, transit cells along the middle part of the crypt axis and differentiated cells at the top of the crypt. In normal colonic crypts the cells renew completely each 3-4 days, through a programmed mechanism which includes the proliferation of cells, their migration along the crypt wall towards the top and their apoptosis, as they reach the top and the cell cycle is finished. If this programmed mechanism changes, disease may appear: the shape of the crypts change and they become aberrant crypts. These have much more cells than normal crypts and aggregate in foci. In conclusion, we can say crypts become aberrant because of the deregulated mechanism of their cells dynamics.

It is well accepted in the scientific community that the dynamics of cells follow logistic type differential equations, which take into account the fact that a growing population will reach a threshold if all the available resources are consumed and the environment does not support any more individuals. Therefore, it seems appropriate to use logistic type equations to model the evolution of the number of ACF because, in the long run, ACF are, in a certain sense, commanded and directed by the cells' populations which reside inside the aberrant crypts. Analogously, it is also reasonable to use logistic type equations to model the behaviour of the apoptosis and proliferation indices in ACF.

In the literature, a reasonable collection of articles concerning the mathematical modelling of cell populations in individual colonic crypts can be found, as well as works dealing with the mathematical modelling of colorectal cancer and, more generally, of tumor growth. We refer, in particular, to [4], [9], [11], [15], [19], [20], [26], [27] and [37] for models concerning dynamics of cell populations, to [5], [13], [17], [20], [21], [23], [32] and [38] for papers

reporting models related to colorectal cancer, to [1], [3], [22], [25], [28], [30], [31] and [34] for the mathematical modelling of tumor growth, and finally to [16], [18], [29], [33], [35] and [36] for medical papers related to ACF and colorectal cancer. To the best of our knowledge, there are very few works reporting the mathematical modelling of ACF in the literature (we have only found [2] and [8]) and none that uses logistic models for ACF. In the article [8], which is somehow related to the present paper, exponential growth equations are used to model the dynamics of normal crypts and two subpopulations of ACF (one consisting of foci with only one aberrant crypt and the other with foci with more than two crypts).

The structure of the paper is the following: after this introduction, we describe the logistic type model for the dynamics of ACF in the human colon, and derive some of its properties in an abstract setting. Then, in section 3, we apply these results to specific clinical examples using available medical data. We report on the conclusions inferred with the models and comment on how they can be used for screening purposes. Finally, in the last section, we summarize the main results of the paper and discuss the possibility of using more involved logistic type differential equations, that could lead to a more accurate mathematical modelling of ACF.

2. The mathematical model

We assume the aberrant crypt foci (ACF, for short) population is split into two disjoint subpopulations, ACF_1 and ACF_2, according to a predefined medical classification (see section 3 for examples and details). We represent by $F_1(t)$ and $F_2(t)$ the number of foci in ACF_1 and ACF_2, respectively, at time t.

We propose that the evolution in time of the populations ACF_1 and ACF_2 is described by the following system of logistic type differential equations (see, $e.g.$, [10], [12], [24])

$$
\begin{cases}
F_1'(t) = k_1\, F_1(t) \left(1 - \dfrac{F_1(t)}{\lambda_1}\right) \\[2ex]
F_2'(t) = k_2\, F_2(t) \left(1 - \dfrac{F_2(t)}{\lambda_2}\right).
\end{cases}
\tag{1}
$$

The parameters k_1, k_2, λ_1 and λ_2 are strictly positive constants: k_1 and k_2 represent the intrinsic growth rates of the populations ACF_1 and ACF_2, respectively, while λ_1 and λ_2 are the carrying capacities of F_1 and F_2. Moreover, we remark that the negative terms $-k_1\frac{F_1(t)^2}{\lambda_1}$ and $-k_2\frac{F_2(t)^2}{\lambda_2}$ can be understood as competition terms from individuals of the species F_1 and F_2, respectively, which compete for the same resources. In the model (1) all these parameters are unknown.

Each of the equations in (1) is a first-order ordinary differential equation involving two parameters, known in the literature as a logistic equation. The solution is well-known, depends on both parameters and the initial condition, and is given by

$$F_i(t) = \frac{\lambda_i\, F_i(0)}{F_i(0) + (\lambda_i - F_i(0))\, e^{-k_i t}}, \qquad i = 1, 2. \tag{2}$$

The functions $F_i(t)$ are positive (since the initial condition is the number of foci at the initial time, a positive number) and monotone, being increasing or decreasing depending on whether $\lambda_i > F_i(0)$ or $\lambda_i < F_i(0)$ (when $\lambda_i = F_i(0)$ the function is constant and equal to λ_i). Their asymptotic profiles are given by

$$F_i(+\infty) := \lim_{t\to+\infty} F_i(t) = \lambda_i, \qquad i = 1, 2, \tag{3}$$

where the λ_i are the carrying capacities.

Our next aim is to express the values of the parameters λ_i in terms of $F_i(0)$, $F_i(1)$ and $F_i(2)$, i.e., in terms of three evaluations of F_i at the equidistant times $t = 0$, $t = 1$ and $t = 2$. From (2), we easily obtain, evaluating F_i at $t = 1$,

$$k_i = -\ln\left(\frac{F_i(0)\,[\lambda_i - F_i(1)]}{F_i(1)\,[\lambda_i - F_i(0)]}\right) \tag{4}$$

Since F_i is a monotone function converging to λ_i, the right hand side in (4) is well defined because the fraction is positive and less than 1. Introducing now the value of the parameter k_i in the expression of $F_i(t)$ given by (2), we obtain

$$F_i(t) = \frac{\lambda_i\, F_i(0)}{F_i(0) + (\lambda_i - F_i(0))\left(\frac{F_i(0)\,[\lambda_i - F_i(1)]}{F_i(1)[\lambda_i - F_i(0)]}\right)^t}. \tag{5}$$

Evaluating now at $t = 2$, we can express the parameter λ_i as a function of $F_i(0)$, $F_i(1)$ and $F_i(2)$ as follows

$$
\lambda_i = \frac{F_i(0) \, F_i(1)^2 + F_i(1) \, F_i(2) \, [F_i(1) - 2 \, F_i(0)]}{F_i(1)^2 - F_i(0) \, F_i(2)}
$$

(6)

$$
= \frac{[F_i(0) - F_i(1)]^2 \, F_i(2) + F_i(0) \, [F_i(1)^2 - F_i(0) \, F_i(2)]}{F_i(1)^2 - F_i(0) \, F_i(2)}, \qquad i = 1, 2.
$$

The domain of the function λ_i, for $i = 1, 2$, is defined by the set of all points $(F_i(0), F_i(1), F_i(2)) \in \mathbb{R}^3_+$ such that $F_i(1)^2 - F_i(0) \, F_i(2) \neq 0$, $\lambda_i > 0$ and $F_i(0) < F_i(1) < F_i(2) < \lambda_i$ if F_i is a monotone increasing function or $F_i(0) > F_i(1) > F_i(2) > \lambda_i$ if F_i is a monotone decreasing function. Equivalently, it can be shown that it is the set

$$
\left\{ (F_i(0), F_i(1), F_i(2)) \in \mathbb{R}^3_+ \ : \ \frac{F_i(0) \, F_i(1)}{2 \, F_i(0) - F_i(1)} < F_i(2) < F_i(1) < F_i(0) \right\} \quad (7)
$$

if F_i is a monotone decreasing function; or the set

$$
\left\{ (F_i(0), F_i(1), F_i(2)) \in \mathbb{R}^3_+ \ : \ F_i(0) < F_i(1) < F_i(2) < \frac{F_i(1)^2}{F_i(0)} \right\} \quad (8)
$$

if F_i is a monotone increasing function.

Notice that λ_i is a monotone function in each of its three variables because the partial derivatives with respect to $F_i(0)$, $F_i(1)$ and $F_i(2)$ satisfy

$$
\frac{\partial \lambda_i}{\partial F_i(0)} = \left(\frac{F_i(1) \, [F_i(1) - F_i(2)]}{F_i(1)^2 - F_i(0) \, F_i(2)} \right)^2 > 0
$$

$$
\frac{\partial \lambda_i}{\partial F_i(1)} = -\frac{2 F_i(0) \, F_i(2) \, [F_i(0) - F_i(1)] \, [F_i(1) - F_i(2)]}{[F_i(1)^2 - F_i(0) \, F_i(2)]^2} < 0 \quad (9)
$$

$$
\frac{\partial \lambda_i}{\partial F_i(2)} = \left(\frac{F_i(1) \, [F_i(1) - F_i(0)]}{F_i(1)^2 - F_i(0) \, F_i(2)} \right)^2 > 0.
$$

3. Auxiliary diagnosis models

In this section, we use the abstract results of the previous section to show how it is possible, by means of model (1), to predict the number of ACF and/or to quantify some of their characteristics and behavior, for a large time t. We choose particular medical criteria and use available medical data

for the test examples. Although we use mean values in the examples, the analysis presented here must be implemented for each individual patient. In particular, each patient has his/her own graphs.

3.1. Percentages of ACF's subpopulations. In this example we split the ACF population into two disjoint sets, ACF_1 and ACF_2, such that the index of proliferative cells (PI for short) is larger or smaller or equal than the PI of the colon normal mucosa. Then

- $F_1(t)$ is the total number of clusters of aberrant crypts of type ACF_1 at time t;
- $F_2(t)$ is the total number of clusters of aberrant crypts of type ACF_2 at time t.

We assume the initial conditions are $F_1(0) = F_2(0) = 1$ and perform one clinical observation at time $t = 1$. We take, using [14], p. 186, table 30,

$$F_1(1) = 10 \qquad \text{and} \qquad F_2(1) = 16. \tag{10}$$

Then, the expressions of $F_1(t)$ and $F_2(t)$ in (5), are given by

$$F_1(t) = \frac{\lambda_1}{1 + (\lambda_1 - 1)\left(\frac{\lambda_1 - 10}{10(\lambda_1 - 1)}\right)^t} \; ; \qquad F_2(t) = \frac{\lambda_2}{1 + (\lambda_2 - 1)\left(\frac{\lambda_2 - 16}{16(\lambda_2 - 1)}\right)^t} \; ,$$

and the carrying capacities defined in (6) are now equal to

$$\lambda_1 = \frac{100 + 80F_1(2)}{100 - F_1(2)}, \quad \text{for} \quad 10 < F_1(2) < 100$$

$$\tag{11}$$

$$\lambda_2 = \frac{256 + 224F_2(2)}{256 - F_2(2)}, \quad \text{for} \quad 16 < F_2(2) < 256.$$

Observe that, according to the values at $t = 0$ and $t = 1$, we are in the case of monotone increasing functions F_i so the domains of the λ_i are given by (8).

We now consider the ratio $\frac{\lambda_1}{\lambda_1 + \lambda_2}$ as a function of the pair $(F_1(2), F_2(2))$. This fraction represents the percentage of ACF_1 in the overall population of ACF for a large time. We express it as a function of the number of ACF_1 and ACF_2 at the future time $t = 2$. The corresponding surface and contour plots are depicted in figure 1. For instance, if at time $t = 2$ we have $(F_1(2), F_2(2)) = (85, 40)$, so the number of ACF_1 is larger than twice the number of ACF_2 at time $t = 2$, then the graphs in figure 1 show that,

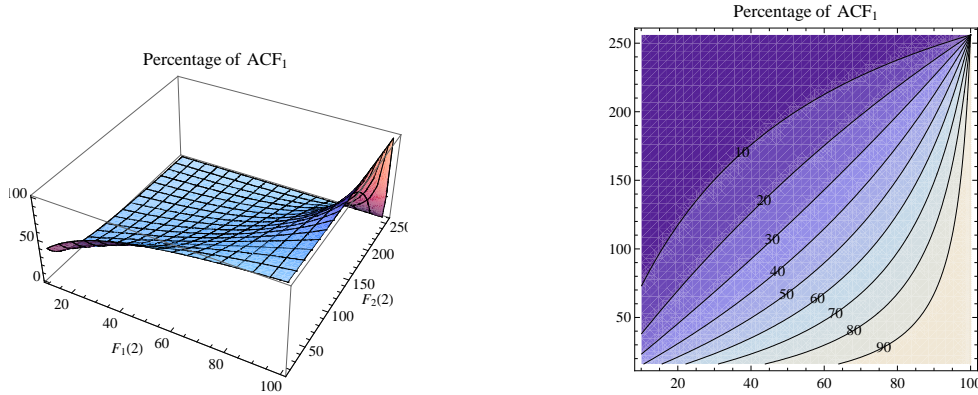for large time, the percentage of ACF_1 in the overall population of ACF is approximately equal to 90%.

FIGURE 1. Percentage of ACF_1 in the overall population of ACF, at a large time t, as a function of the number of ACF_1 and ACF_2 at the future time $t = 2$; surface plot (left) and contour plot (right).

We notice that the function $\frac{\lambda_1}{\lambda_1+\lambda_2}$ is monotone increasing with respect to the variable $F_1(2)$, but it is monotone decreasing with respect to $F_2(2)$. In fact, because of the third formula in (9), the partial derivatives verify

$$\frac{\partial \frac{\lambda_1}{\lambda_1+\lambda_2}}{\partial F_1(2)} = \frac{\lambda_2}{(\lambda_1+\lambda_2)^2}\frac{d\lambda_1}{dF_1(2)} > 0 \quad \text{and} \quad \frac{\partial \frac{\lambda_1}{\lambda_1+\lambda_2}}{\partial F_2(2)} = \frac{-\lambda_1}{(\lambda_1+\lambda_2)^2}\frac{d\lambda_2}{dF_2(2)} < 0.$$

This monotonicity property can be observed in figure 1: if $F_1(2) = 40$, for example, the graphs show that the percentage $\frac{\lambda_1}{\lambda_1+\lambda_2}$ decreases as the number of ACF_2 at time $t = 2$ increases. On the other hand, if $F_2(2) = 60$, the percentage increases as the number of ACF_1 at time $t = 2$ increases.

A similar analysis can be performed using instead the index of apoptotic cells. The combination of the input given by the analysis of both cases, namely the data available from the graphs, might be very useful for doctors for the identification of a possible risk situation. This would be so, in particular, if the occurrence of cancer could be related to the number of ACF classified according to the order of magnitude of their PI and AI with respect to PI and AI of the normal mucosa.

3.2. Extrapolating from one clinical observation. In this example, and in contrast to the previous one, we do not count the number of ACF. Our objective is to describe the possible values of the AI in ACF for a large time

t, based on only one clinical observation and assuming this index follows a logistic type law. This is a reasonable assumption since this type of indices are defined from counting the number of cells with a certain property. The same type of analysis can be performed for the AI in the normal mucosa (NM for short) or for the PI in ACF or in the NM.

We use medical data concerning four groups of patients: with adenomatous polyps (group A), with carcinoma (group B), without lesions in the colon (group C) and with non-adenomatous polyps (group D). We set for time $t = 0$ the following mean values, taken from [14, p.181, table 26]:

values of AI at $t = 0$	A	B	C	D
ACF	1.8	1.1	2.2	1.7
NM	1.5	2.0	2.0	2.1

values of PI at $t = 0$	A	B	C	D
ACF	8.6	10.0	11.3	11.4
NM	8.9	9.5	11.2	7.5

We analyze only one case but it is possible to compare what happens in the sixteen different scenarios.

Let $F(t)$ represent the AI in ACF at time t for a patient with carcinoma (class B). Assume, according to the table, that $F(0) = 1.1$. We will describe all the possible values of the carrying capacity λ (*i.e.*, the asymptotic value of the AI as t is large) as a function of two future clinical observations at equidistant times, say as a function of $F(1)$ and $F(2)$. According to (6), we have

$$\lambda = \frac{1.1 \times F(1)^2 + F(2)\left[F(1)^2 - 2.2 \times F(1)\right]}{F(1)^2 - 1.1 \times F(2)}.$$

The behaviour of this function depends dramatically on wether F is decreasing or increasing, its domains of definition being respectively (see (7) and (8))

$$0 < \frac{1.1 \times F(1)}{2.2 - F(1)} < F(2) < F(1) < 1.1$$

and

$$1.1 < F(1) < F(2) < \frac{F(1)^2}{1.1}.$$

The graphs in figure 2 will become an effective diagnosis tool once a critical threshold value for the AI is established. Suppose, for instance, that there is strong medical evidence suggesting that values of the AI in ACF under a yet unknown cut-off are linked to a significant increased risk of colorectal cancer in the future. After the two further clinical observations, the analysis of the
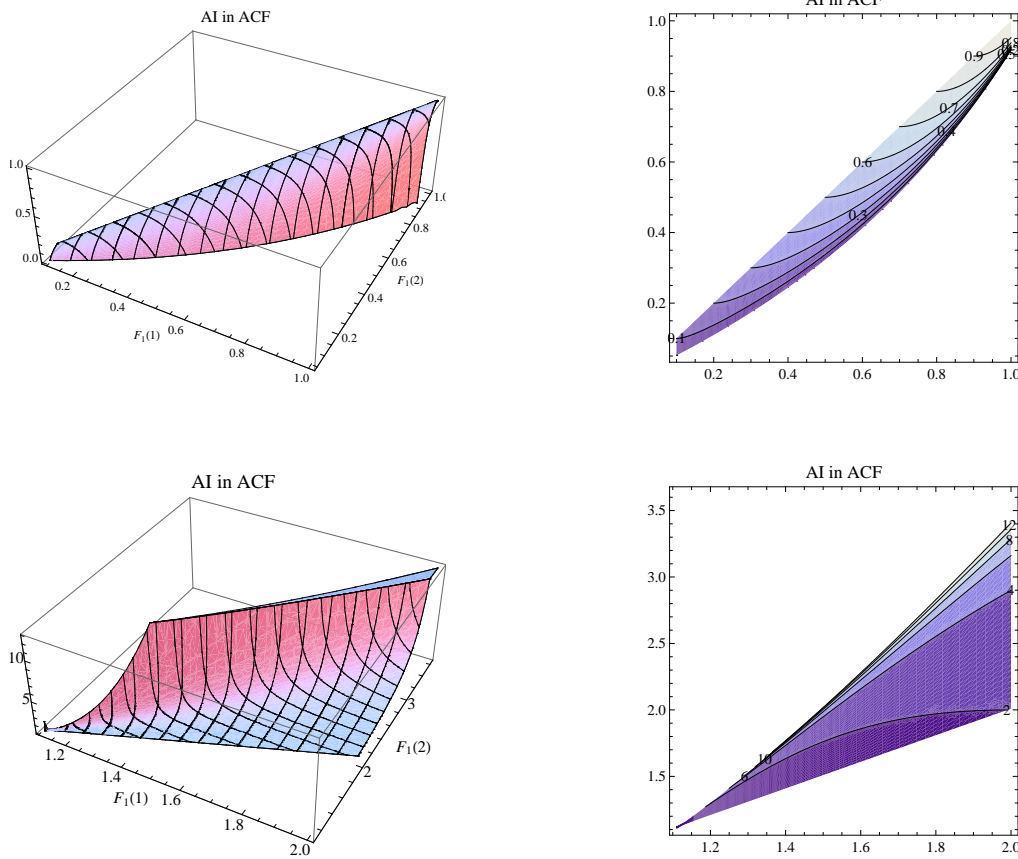
FIGURE 2. AI in ACF for a patient of group B, at a large time t, as a function of $F(1)$ and $F(2)$, and when F is monotone decreasing (top) and monotone increasing (bottom): surface plots (left) and contour plots (right).

graphs can help screening the patients condition and immediately establish if the situation is of increased risk or not. Note that the function λ is decreasing as a function of $F(1)$ and increasing as a function of $F(2)$, in accordance with the abstract analysis of section 2 (cf. the second and third equations in (9)).

3.3. Ratio between indices. It can also be of interest to have available the possible values of the ratio between the indices (AI or PI) in ACF and the NM. Let us consider the PI in a patient with carcinoma (class B), with $F_1(t)$ and $F_2(t)$ representing, respectively, the PI in AFC and the PI in the NM at time t. Moreover, we now take two medical observations:

- at time $t = 0$, we use the mean values of the PI for a patient without lesions; according to the table, $F_1(0) = 11.3$ and $F_2(0) = 11.2$;

- at time $t = 1$, we use the mean values in the table for a patient of
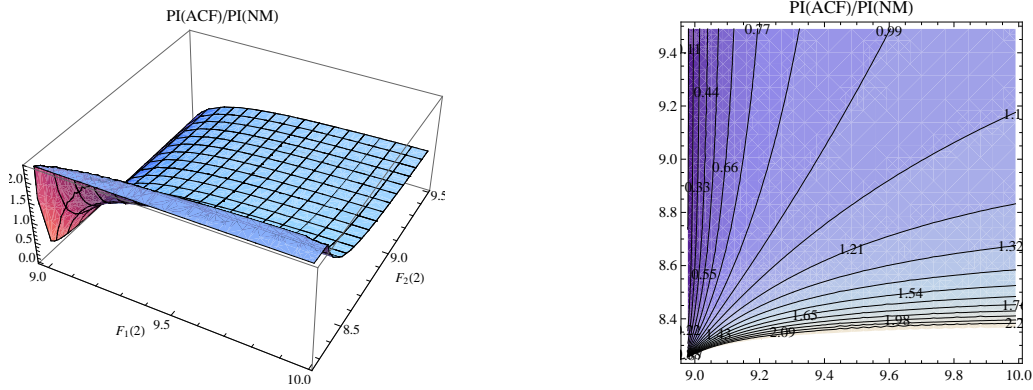 class B, namely $F_1(1) = 10.0$ and $F_2(1) = 9.5$.

FIGURE 3. Ratio of the PI in ACF and in the NM, at a large time t, for a patient in group B: surface plot (left) and contour plot (right).

We then have the carrying capacity λ_1 (representing the value of the PI in ACF for large t) as a function of $F_1(2)$ and the carrying capacity λ_2 (representing the value of the PI in the NM for large t) as a function of $F_2(2)$. Again using (6), the ratio is then given by

$$\frac{\lambda_1}{\lambda_2} = \frac{\dfrac{10^2 \times 11.3 + \left[10^2 - 2 \times 11.3 \times 10\right] F_1(2)}{10^2 - 11.3\, F_1(2)}}{\dfrac{9.5^2 \times 11.2 + \left[9.5^2 - 2 \times 9.5 \times 11.2\right] F_2(2)}{9.5^2 - 11.2\, F_2(2)}}$$

and defined, since F_1 and F_2 are decreasing, for

$$8.97 \approx \frac{11.3 \times 10}{2 \times 11.3 - 10} < F_1(2) < 10$$

and

$$8.25 \approx \frac{11.2 \times 9.5}{2 \times 11.2 - 9.5} < F_2(2) < 9.5 \ .$$

The interest of the graphs displayed in figure 3 is the possibility of easily assessing, at the third medical observation at time $t = 2$, if the corresponding ratio represents a risk for the patient. For example, if this leads us close to the line where the ratio is equal to one in the contour plot, we may conclude the PI's in ACF and the NM will be asymptotically very similar, arguably an indication that there is no risk. Likewise, a very large ratio in the case of

the PI or a very small ratio in the case of the AI could be a clear indication that the adequate screening medical procedures should be implemented.

3.4. Predicting the effect of a drug agent. This example is somehow related to example 3.2 but now we extrapolate from two medical observations. The aim is to compare, for a large time t, the value of AI and PI in ACF and in the NM.

Using the AI and PI measured in ACF and NM, we also predict what is the effect of a drug administrated in ACF and NM, in a trial that involves two medical observations. With this in mind, the group of patients of class A, defined in example 3.2, is divided in two subgroups with the same number of individuals. During a fixed period of time, the drug is administrated to one subgroup of patients and a placebo to the other subgroup. The AI and PI are measured in each subgroup, both in ACF and in the NM, before and after the administration of the drug or the placebo. Thus, for this example,

- $F_1(t)$ is the AI (or the PI) in ACF at time t,
- $F_2(t)$ is the AI (or the PI) in the NM at time t.

We use the following data, available from [14, p.202, fig.22]. It represents the values of AI and PI, for the two subgroups of patients, in ACF and in the NM, measured before $(t = 0)$ and after $(t = 1)$ the administration of the placebo and the drug.

administration of placebo				administration of drug		
AI	$F_1(t)$	$F_2(t)$		AI	$F_1(t)$	$F_2(t)$
$t = 0$	2.1	1.2		$t = 0$	1.7	1.6
$t = 1$	1.1	1.6		$t = 1$	2.6	2.3
PI	$F_1(t)$	$F_2(t)$		PI	$F_1(t)$	$F_2(t)$
$t = 0$	9.7	10.3		$t = 0$	8.2	8.7
$t = 1$	11.2	7.1		$t = 1$	5.5	8.2

The curves plotted in figures 4 and 5 show the values of AI and PI, respectively, for a large time t. They correspond to the values of the carrying capacities λ_1 and λ_2, as functions of $F_1(2)$ and $F_2(2)$, respectively, for the two subgroups of patients, and for the two types of sample tissues, ACF and NM.

From figure 4 we conclude that, for a large time t, the AI in ACF, for the patients who have taken the placebo, is significantly smaller than the AI in ACF for the patients who have taken the drug (compare the two graphs of
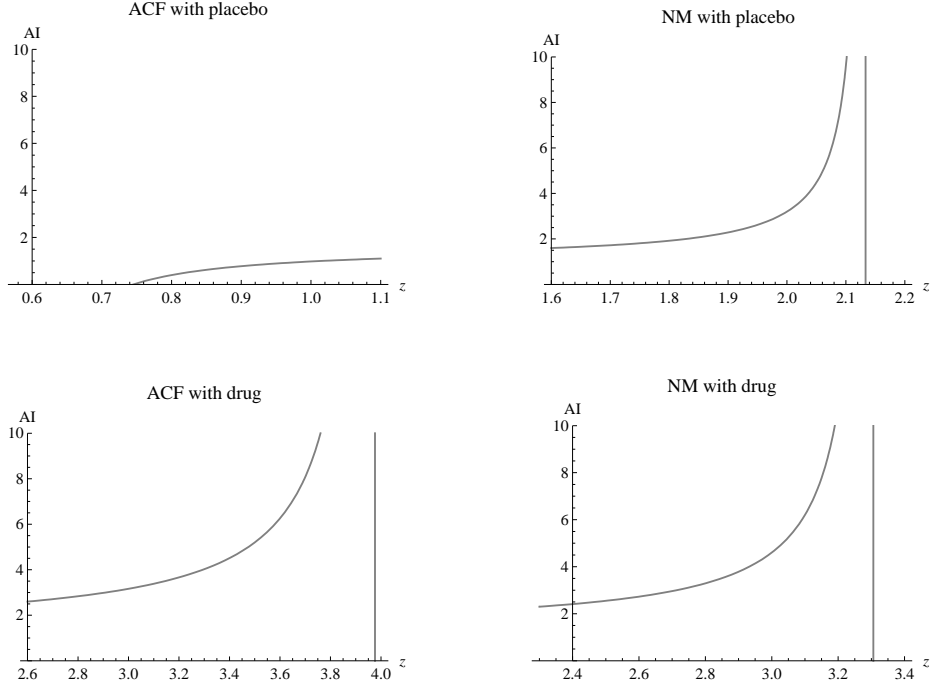
FIGURE 4. Values of AI in ACF and NM with placebo (top) and drug (bottom), for a large time t: $\lambda_1 = \frac{2.541-3.41z}{1.21-2.1z}$ and $1.1 > z > 0.745161$ (top left), $\lambda_2 = \frac{3.072-1.28z}{2.56-1.2z}$ and $1.6 < z < 2.13333$ (top right), $\lambda_1 = \frac{11.492-2.08z}{6.76-1.7z}$ and $2.6 < z < 3.97647$ (bottom left), $\lambda_2 = \frac{8.464-2.07z}{5.29-1.6z}$ and $2.3 < z < 3.30625$ (bottom right), with $z = F_i(2)$ for $i = 1, 2$.

the left column in figure 4). This means that the drug has a positive effect since an increase of the AI in ACF possibly indicates a reduction of ACF carcinogenic potential. Moreover, the curves in the top right and bottom left graphs of figure 4 are somehow similar, which shows the AI in ACF for the patients with drug tend to have the same values as the AI in the NM for the patients with placebo. On the other hand, the effect of the placebo and the drug in the AI of the NM seems to be similar for the two groups of patients (see the two graphs of the right column in figure 4).

By analyzing the graphs in figure 5, we infer that, at a large time t, the placebo and the drug have a similar effect in terms of the PI of the NM in the two groups of patients (see the two graphs of the right column in figure 5). In contrast, this effect is very different in the PI of ACF (compare the two graphs of the left column in figure 5): for the patients who have received placebo the PI can achieve the value 22 (which is the value in carcinoma,
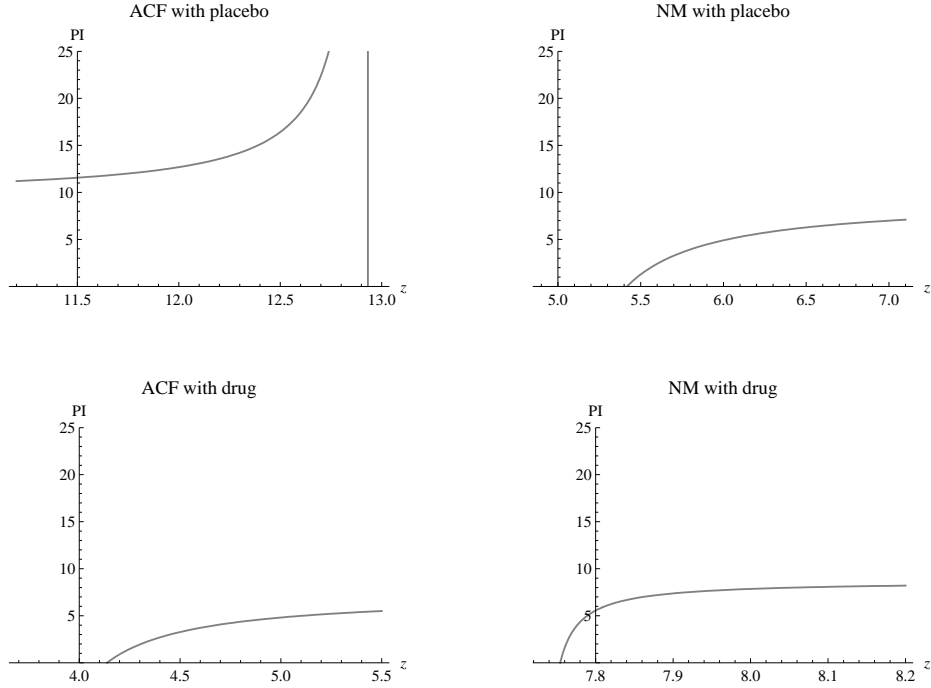
FIGURE 5. Values PI in ACF and NM with placebo (top) and drug (bottom), for a large time t: $\lambda_1 = \frac{1216.77-91.84z}{125.44-9.7z}$ and $11.2 < z < 12.932$ (top left), $\lambda_2 = \frac{519.223-95.85z}{50.41-10.3z}$ and $7.1 > z > 5.41704$ (top right), $\lambda_1 = \frac{248.05-59.95z}{30.25-8.2z}$ and $5.5 > z > 4.13761$ (bottom left), $\lambda_2 = \frac{584.988-75.44z}{67.24-8.7z}$ and $8.2 > z > 7.75435$ (bottom right), with $z = F_i(2)$ for $i = 1, 2$.

see [14], p.187, table 32), while for those who have taken the drug the PI is much smaller, comparable to the value of PI in the NM with placebo (see the top right graph in figure 5), and never reaches such high values as 22.

4. Conclusions and future work

In this paper, logistic mathematical models are proposed for the growth dynamics of aberrant crypt foci in the human colon. These models predict the number of ACF at a large time and quantify the AI and the PI in ACF, as functions of one or two unknown clinical observations. This type of information, specially if appropriately combined, might be useful for doctors as an auxiliary screening tool.

Other more involved logistic type models could have been considered. For instance, logistic delay models (see [24] and [31]), which might be more realistic for the modelling of ACF because they incorporate a time delay that

would take into account the time required by ACF to develop. Another possibility would be to assume that the two sub-populations of ACF interact, their dynamics being then modeled by a predator-prey model (if the growth rate of one population is decreased and that of the other is increased) or a competition model (if the growth rate of both populations is decreased), or even with a mutualism or symbiosis model (if each population's growth rate is enhanced) (see [24]).

We are aware that these more involved logistic type models could produce more accurate and reliable results, that would also be more consistent with real phenomena and observations when appropriately adjusted and complemented with external medical or biological information. In future work, we intend to pursue along these lines and address more complex issues.

References

[1] T. Alarcón, H. Byrne, and P. Maini. Towards whole-organ modelling of tumour growth. *Progress in Biophysics & Molecular Biology*, 85:451–472, 2004.

[2] T. Apanasovich and al. Aberrant crypt foci and semiparametric modeling of correlated binary data. *Biometrics*, 2007.

[3] R. Araujo and L. McElwain. A history of the study of solid tumour growth: the contribution of mathematical modelling. *Bulletin of Mathematical Biology*, 66(1039–1091), 2004.

[4] N. Armstrong, K. Painter, and J. Sherratt. A continuum approach to modelling cell-cell adhesion. *J Theor. Biol.*, 243:98–113, 2006.

[5] M. Bienz and H. Clevers. Linking colorectal cancer to wnt signaling. *Cell*, 103:311–320, 2000.

[6] R. P. Bird. Role of aberrant crypt foci in understanding the pathogenesis of colon cancer. *Cancer Letters*, 93:55–71, 1995.

[7] R. P. Bird and C. K. Good. The significance of aberrant crypt foci in understanding the pathogenesis of colon cancer. *Toxicology Letters*, 112-113:395–402, 2000.

[8] M. Bjerknes. Expansion of mutant stem cell populations in the human colon. *J. Theor. Biol.*, 178:381–385, 1996.

[9] B. Boman, J. Fields, J. Bonham-Carter, and O. Runquist. Computer modeling implicates stem cell overproduction in colon cancer initiation. *Cancer Research*, 61:8408–8411, 2001.

[10] Gerda de Vries, Thomas Hillen, Mark Lewis, Johannes Müller, and Birgitt Schönfisch. *A course in mathematical biology*, volume 12 of *Mathematical Modeling and Computation*. Society for Industrial and Applied Mathematics (SIAM), Philadelphia, PA, 2006. Quantitative modeling with mathematical and computational methods.

[11] D. Drasdo and M. Loeffer. Individual-based models to growth and folding in one-layered tissues: intestinal crypts and early development. *Nonlinear Analysis*, 47:245–256, 2001.

[12] Leah Edelstein-Keshet. *Mathematical models in biology*, volume 46 of *Classics in Applied Mathematics*. Society for Industrial and Applied Mathematics (SIAM), Philadelphia, PA, 2005. Reprint of the 1988 original.

[13] C. Edwards and S.J. Chapman. Biomechanical modelling of colorectal crypt budding and fission. *Bulletin of Mathematical Biology*, to appear, 2007.

[14] Pedro M. N. Figueiredo. *Focos de criptas aberrantes: contribuição para o estudo da sua relação com a carcinogénese colo-rectal, uma investigação clínica, endoscópica e laboratorial.* Faculdade de Medicina, Universidade de Coimbra, Portugal, 2006. PhD Thesis (in Portuguese).

[15] J. Galle, M. Loeffler, and D. Drasdo. Modeling the effect of deregulated proliferation and apoptosis on the growth dynamics of epithelial cell populations in vitro. *Biophysical Journal*, 88:62–75, 2005.

[16] L. Greaves and al. Mitochondrial dna mutations are established in human colonic stem cells, and mutated clones expand by crypt fission. *PNAS*, 103(3):714–719, 2006.

[17] P. Harper and S. Jones. Mathematical models for the early detection and treatment of colorectal cancer. *Health Care Management Science*, 8:101–109, 2005.

[18] D. Hurlstone and al. Rectal aberrant crypt foci identified using high-magnification-chromoscopic colonoscopy: biomarkers for flat and depressed neoplasia. *American Journal of Gastroenterology*, pages 1283–1289, 2005.

[19] M. Johnston, C. Edwards, W. Bodmer, P. Maini, and S.J. Chapman. Mathematical modeling of cell population dynamics in the colonic crypt in colorectal cancer. *PNAS*, 104(10):4008–4013, 2007.

[20] I. Leeuwen, H. Byrne, O. Jensen, and J. King. Crypt dynamics and colorectal cancer: advances in mathematical modelling. *Cell Prolif.*, 39:157–181, 2006.

[21] I. Leeuwen, C. Edwards, M. Ilyas, and H. Byrne. Towards a multiscale model of colorectal cancer. *World J Gastroenterol*, 13(9):1399–1407, 2007.

[22] N. Mantzaris, S. Webb, and H. Othmer. Mathematical modeling of tumor-induced angiogenesis. *J. Math. Biol.*, 49:111–187, 2004.

[23] F. Michor, Y. Iwasa, C. Lengauer, and M. Nowak. Dynamics of colorectal cancer. *Seminars in Cancer Biology*, 15:484–494, 2005.

[24] J. D. Murray. *Mathematical biology: I. An Introduction*, volume 17 of *Interdisciplinary Applied Mathematics: Mathematical Biology*. Springer-Verlag, Berlin, 2002.

[25] J. D. Murray. *Mathematical biology: II. Spatial Models and Biomedical Applications*, volume 18 of *Interdisciplinary Applied Mathematics: Mathematical Biology*. Springer-Verlag, Berlin, 2004.

[26] A. Onofrio and I. Tomlinson. A nonlinear mathematical model of cell turnover, differentiation and tumorigenesis in the intestinal crypt. *J. theor. Biol.*, 244:367–374, 2007.

[27] U. Paulus and al. The differentiation and lineage development of goblet cells in the murine small intestinal crypt: experimental and modelling studies. *Journal of Cell Science*, 106:473–484, 1993.

[28] P. Pinsky. A multi-stage model of adenoma development. *J. theor. Biol.*, 207:129–143, 2000.

[29] S. Preston and al. Bottom-up histogenesis of colorectal adenomas: Origin in the monocryptal adenoma and initial expansion by crypt fission. *Cancer Research*, 63:3819–3825, 2003.

[30] L. Preziosi and A. Farina. On darcy's law for growing porous media. *International Journal of Non-Linear Mechanics*, 37:485–491, 2002.

[31] A. Quarteroni, L. Formaggia, and A. Veneziani. *Complex systems in Biomedicine*. Springer-Verlag Italia, Milano, 2006.

[32] B. Ribba, T. Colin, and S. Schnell. A multiscale mathematical model of cancer, and its use in analyzing irradiation therapies. *Theor Biol Med Model.*, (3:7), 2006.

[33] L. Roncucci, A. Medline, and W. Bruce. Classification of aberrant crypt foci and microadenomas in human colon. *Cancer Epidemiology, Biomarkers & Prevention*, 1:57–60, 1991.

[34] J. Sherratt and M. Chaplain. A new mathematical model for avascular tumour growth. *J. Math. Biol.*, 43:291–312, 2001.

[35] I-M. Shih and al. Top-down morphogenesis of colorectal tumors. *PNAS*, 98(5):2640–2645, 2001.

[36] R. Taylor and al. Mitochondrial dna mutations in human colonic crypt stem cells. *J. Clin. Invest.*, 112(9):1351–1360, 2003.

[37] I. Tomlinson and W. Bodmer. Failure of programmed cell death and differentiation as causes of tumors: some simple mathematical models. *PNAS*, 92(9):11130–11134, 1995.

[38] D. Wodarz. Effect of stem cell turnover rates on protection against cancer and aging. *J. theor. Biol.*, 245:449–458, 2007.

Isabel N. Figueiredo
CMUC, Department of Mathematics, University of Coimbra, 3001-454 Coimbra, Portugal

E-mail address: isabelf@mat.uc.pt

Pedro N. Figueiredo
Faculty of Medicine, University of Coimbra and Department of Gastroenterology, University Hospital of Coimbra, 3000-075 Coimbra, Portugal

E-mail address: pedro.n.figueiredo@clix.pt

Carlos Leal
CMUC, Department of Mathematics, University of Coimbra, 3001-454 Coimbra, Portugal

E-mail address: carlosl@mat.uc.pt

José Miguel Urbano
CMUC, Department of Mathematics, University of Coimbra, 3001-454 Coimbra, Portugal

E-mail address: jmurb@mat.uc.pt